

# Nonlocal Phonon Heat Transport Seen in 1-d Pulses

Philip B. Allen\* and Nhat A. Nghiem

Department of Physics and Astronomy, Stony Brook University, Stony Brook, NY 11794-3800, USA

(Dated: September 20, 2022)

Propagation of vibrational energy from an initial localized pulse gives useful insights into non-local phonon transport. We report simulations in one dimension. The 1d case has tricky anomalies, but provides the simplest pictures of the evolution from initially ballistic toward longer time diffusive propagation. Our results show interesting details, such as diverse results from different definitions of atomistic local energy, and failure to exhibit pure diffusion at long times. Boltzmann phonon gas theory, including external energy insertion, is applied to this inherently time-dependent and nonlocal problem. The solution, using relaxation time approximation for impurity scattering, does not closely agree with the simulated results.

## I. INTRODUCTION

Figure 1 shows the local energy at atom sites on a one-dimensional harmonic chain of  $N = 200$  atoms with periodic boundary conditions. At time  $t = 0$ , the chain is in its ground state. An infinitesimal time later, one or two central atoms are disturbed. The pulse propagates classically. There are two main points of this paper. (1) To gain insight into the “crossover” from the ballistic propagation of Fig. 1 toward diffusive heat propagation when phonons start to evolve toward a local equilibrium  $T(r, t)$  because of scattering<sup>1</sup>. (2) To test the form and the accuracy of a non-local Boltzmann equation description<sup>2</sup>.

The chain has atoms of mass  $M = 1$  separated by distance  $a = 1$  and connected by springs of constant  $K = 1$ . The harmonic normal modes have frequency  $\omega_Q = \omega_M \sin(Qa/2)$  where  $\omega_M = 2\sqrt{K/M} = 2$ . Time is measured in units  $\sqrt{M/K} = 2/\omega_M = 1$ . The modes propagate at velocities  $v_Q = v_M \cos(Qa/2)\text{sign}(Q)$  where  $v_M = \sqrt{(K/M)a} = 1$ . The unit of energy is  $E_0 = 1 = Ka^2 = Mv_M^2 = M\omega_M^2 a^2/4$ . The leading edges of the pulse propagate at the speed of sound,  $\pm v_M = \pm 1$ , as is seen at  $t = 30$  in Fig. 1.

The Hamiltonian of the chain is

$$\mathcal{H} = \sum_{\ell} \left[ \frac{P_{\ell}^2}{2M} + \frac{1}{2}K(u_{\ell} - u_{\ell+1})^2 \right]. \quad (1)$$

Atoms have displacements  $u_{\ell}$  around average positions  $r_{\ell} = \ell a$ . The general solution of Newton’s equations of motion is

$$u_{\ell}(t) = \sqrt{\frac{1}{N}} \sum_Q A_Q \cos(Q\ell a - \omega_Q t + \phi_Q), \quad (2)$$

There are  $2N$  free parameters, amplitude  $A_Q \geq 0$  and phase  $\phi_Q$  for each normal mode  $Q$ . The wavevector has the form  $Q = (2\pi/a)(n/N)$ , and the integer  $n$  lies in the range  $-N/2 < n \leq N/2$ . The pulses shown in Fig. 1, labeled D, V2, and V1, are generated by initial disturbances given in Table I. The “V1” (or “velocity”) pulse has only the central atom given a velocity  $v_0$  at  $t = 0$ . The “V2” (or “dual velocity”) pulse has two central atoms given equal and opposite velocities. The “D”

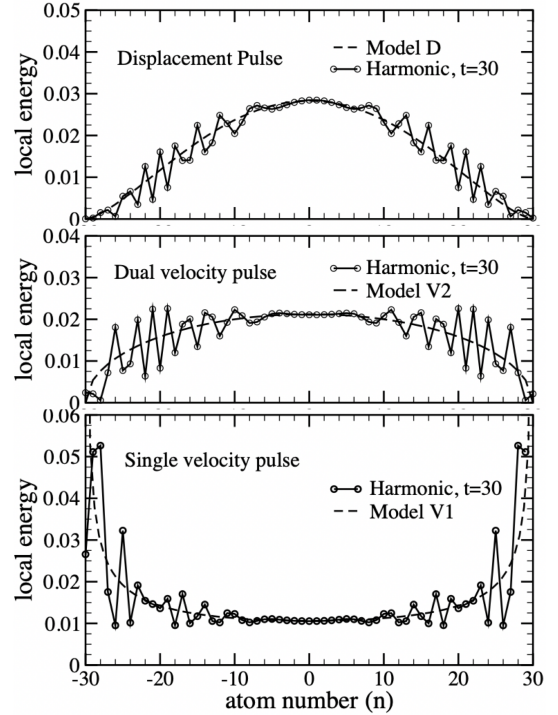


FIG. 1. Circles connected by solid lines are the computed local energy  $E_a(\ell)$  at  $t = 30$  for three types of pulses (see Eq. 3 and Table I). All three pulses evolve from energy inserted at  $t = 0$  and  $r \sim 0$  into a harmonic chain. The D and V2 pulses are initiated on atoms 0 and 1, but their positions on the horizontal axis are shifted by  $-1/2$  to make them symmetric around  $r = 0$ . The dashed curves are models derived from a continuum picture, such as Boltzmann theory, and given in Eqs. 10, 11, 12.

(or “displacement”) pulse has two central atoms given equal and opposite displacements at  $t = 0$ .

The first result to notice is the interesting diversity of pulse shapes for different initial disturbances. The first issue to resolve is whether local energy is well-defined.

name	$\Delta u_0$	$\Delta u_1$	$\Delta v_0$	$\Delta v_1$
V1	0	0	$\sqrt{2}$	0
V2	0	0	-1	1
D	$-1/\sqrt{3}$	$1/\sqrt{3}$	0	0

TABLE I. Properties of pulses. The shift  $\Delta u$  (in units of  $a$ ) of initial displacement, or  $\Delta v$  (in units of  $v_M$ ) of initial velocity, is scaled so that the new coordinates ( $u_0 + \Delta u_0$ ,  $u_1 + \Delta u_1$ ,  $v_0 + \Delta v_0$ ,  $v_1 + \Delta v_1$ ), of atoms  $\ell = 0$  and 1, have total extra energy equal to  $E_0 = 1$ . The values in the table are the ones that work at  $T = 0$ , where  $u_0 = 0$ , *etc.*

## II. DEFINING LOCAL ENERGY

Local energy  $E(\ell, t)$  cannot be unambiguously defined. In classical physics it should obey  $\sum_{\ell} E(\ell, t) = \mathcal{H}$ . The version plotted in Fig. 1 is defined as

$$E_a(\ell, t) = \frac{Mv_{\ell}(t)^2}{2} + \frac{K}{4} [(u_{\ell-1}(t) - u_{\ell}(t))^2 + (u_{\ell}(t) - u_{\ell+1}(t))^2]. \quad (3)$$

Each atom is assigned its own kinetic energy, and half of the potential energy of the springs to its left and right. This is a commonly used definition, but is not unique. Two other sensible choices for distributing potential energy to different sites are

$$E_b(\ell) = \frac{Mv_{\ell}^2}{2} + \frac{K}{2} [(2u_{\ell}^2 - u_{\ell}(u_{\ell-1} + u_{\ell+1}))], \quad (4)$$

$$E_c(\ell) = \frac{Mv_{\ell}^2}{2} \text{ and } E_c(\ell + 1/2) = \frac{V}{2}(u_{\ell} - u_{\ell+1})^2. \quad (5)$$

The conventional version  $E_a$  will be used in this paper, but it is interesting to see how it compares with versions  $E_b$  and  $E_c$ , as shown in Fig. 2. The large oscillations seen in version (c) are surprising, and the smoothness seen in version (b) is even more surprising. This diversity illustrates our second result, a well-known fact: local energy at the atom level is not a clear concept. However, if local energy is averaged over a few nearby atoms, it becomes less diverse. The ambiguity also exists in quantum treatments. Marcolongo *et al.*<sup>3</sup> and Ercole *et al.*<sup>4</sup> have shown how this ambiguity does not affect the computation of bulk transport. In the next section we will see that local energy makes more sense in a continuum theory than an atomistic theory.

Figure 1 shows  $E_a(\ell, t)$  for pulses, inserted at  $t = 0$  into zero-temperature (*i.e.* stationary,  $T = 0$ ) chains. Figure 3 shows the same pulse forms, at  $t = 20$ , inserted into chains with a pre-existing thermal distribution of velocities and displacements. In  $T > 0$  cases, the initial pulse amplitudes ( $\Delta u_{0,1}$  or  $\Delta v_{0,1}$ ) are scaled from those in table I to make the total extra energy  $\sum_{\ell} \Delta E_a(\ell)$  of

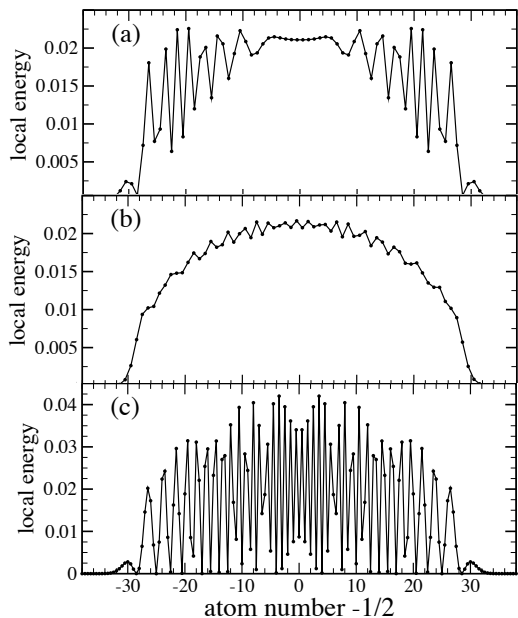


FIG. 2. The harmonic V2 pulse at temperature  $T = 0$  and time  $t = 30$ , using three ways (Eqs. 3-5) of assigning potential energy to a local site energy,  $E(\ell)$ . In (a) and (b), the pulse energy is  $\Delta E = \sum_{\ell} E(\ell)$ . The area under the curves is  $E_0$ , chosen to be 1. In (c), however, the energy has two parts,  $\sum_{\ell} [KE(\ell) + PE(\ell + 1/2)]$ . The values in the graph have been arbitrarily doubled so that the total energy, also 1, is the area under the graph. These graphs demonstrate that the “continuum picture” of energy density (the dashed curves in Fig. 1) is more sensible than these local pictures.

name	Amplitude $A_Q$ from Eq. 6	phase $\phi_Q$	modal energy $\Delta E_Q^{\text{ext}}$
V1	$\frac{\Delta v_0}{\sqrt{N\omega_Q}}$	$\frac{\pi}{2}$	$\frac{E_0}{N}$
V2	$\frac{2\Delta v_0}{\sqrt{N\omega_Q}} \sin\left(\frac{Qa}{2}\right)$	$\pi - \frac{Qa}{2}$	$\frac{2E_0}{N} \sin^2\left(\frac{Qa}{2}\right)$
D	$\frac{2\Delta u_0}{\sqrt{N}} \sin\left(\frac{Qa}{2}\right)$	$-\frac{\pi}{2} - \frac{Qa}{2}$	$\frac{8E_0}{3N} \sin^4\left(\frac{Qa}{2}\right)$

TABLE II. More properties of pulses: the distribution among normal modes  $Q$  of the phonon amplitude  $A_Q$ , phase  $\phi_Q$ , and energy, for the pulses of table I inserted at  $T = 0$ .

all pulses of the ensemble equal to 1. The pulse profiles in Figs. 1 and 3 were computed in two different ways: (1) by numerical integration of Newton’s laws, and (2), by finding the coefficients  $A_Q$  and  $\phi_Q$  in Eq. 2. These coefficients are independent of time, and can be found if the positions  $u_{\ell}$  and velocities  $v_{\ell} = du_{\ell}/dt$  are known at any chosen time:

$$A_Q e^{i(\phi_Q - \omega_Q t)} = \sqrt{\frac{1}{N}} \sum_{\ell} \left[ u_{\ell}(t) + i \frac{v_{\ell}(t)}{\omega_Q} \right] e^{-iQ\ell a}. \quad (6)$$

For the  $T = 0$  case, values of  $A_Q$  and  $\phi_Q$  are given in table II. They are derived from the  $t = 0^+$  positions and velocities shown in table I at  $t = 0$ .

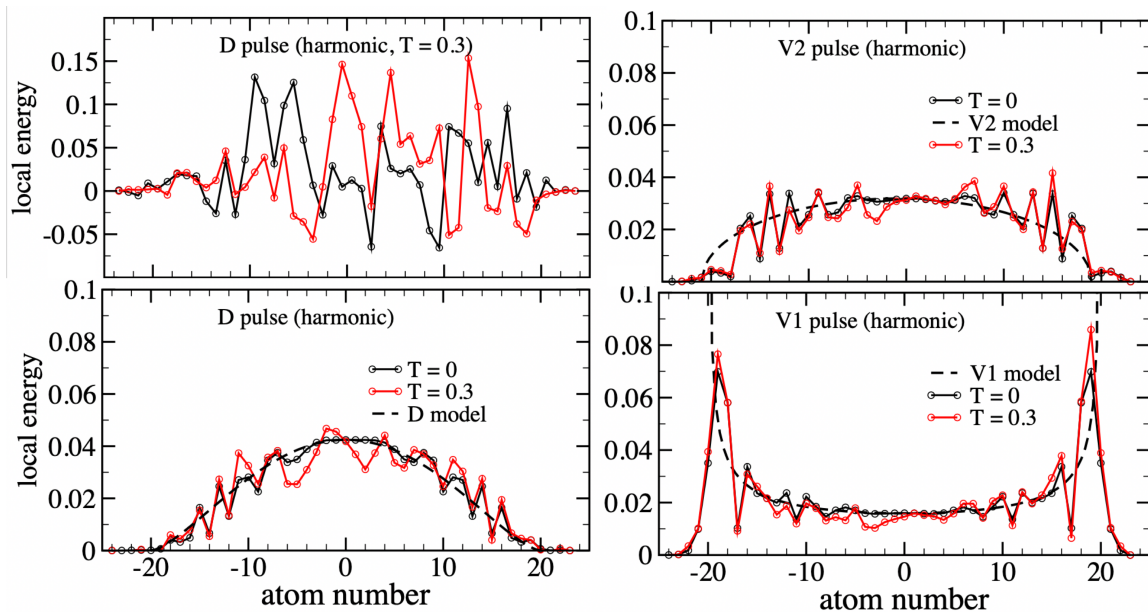


FIG. 3. Pulses of total energy  $\sum_{\ell} \Delta E_{\alpha}(\ell) = E_0 = 1$  at  $t = 20$ , inserted at  $t = 0$  to harmonic chains whose random positions and velocities at  $t = 0^-$  are thermalized at temperature  $T = 0.3$  ( $E_{\text{tot,th}} = 0.3N$ ). The local energies  $\Delta E_{\alpha}(\ell)$  shown in the graphs are the differences between  $E_{\alpha}(\ell, t = 20)$  with and without pulse insertion. The first graph shows D pulses inserted with two typical initial conditions. The other graphs show, in red, the results averaged over 1000-member ensembles with random thermal initial conditions. The black results repeat the zero-temperature pulses shown in Fig. 1. The finite  $T$  pulse shapes, after ensemble averaging, are converging towards the zero-temperature pulse shapes.

The chains are harmonic, so the pulses propagate ballistically. The left or right parts have root mean square (rms) displacements  $\bar{r}$  defined as

$$\bar{r}(t) \equiv \left[ \frac{\sum_{\ell} (\ell a)^2 \Delta E(\ell, t)}{\sum_{\ell} \Delta E(\ell, t)} \right]^{1/2}. \quad (7)$$

The rms displacements increase at speeds  $v_{\text{rms}} = d\bar{r}/dt \approx v_M/\sqrt{n}$ , with  $n = 2, 4, 6$  for the V1, V2, and D pulses, respectively. These values are derived from the continuum description described next.

### III. A CONTINUUM DESCRIPTION

The energy content of each normal mode is

$$E(Q) = \frac{1}{2} M \omega_Q^2 A_Q^2. \quad (8)$$

Using values of  $A_Q$  from Table II, the mode energies are also shown in Table II. A continuum description averages over specific atomic coordinates, and requires a new definition of local energy density  $E(r, t)$ . An appropriate definition for a pulse originating at  $(r, t) = (0, 0)$  is

$$\Delta E(r, t) = \sum_Q \Delta E_Q^{\text{ext}} \delta(r - v_Q t). \quad (9)$$

After integrating over  $Q$ , the results for the three pulses are

$$\Delta E_{V1}(r, t) = \frac{E_0}{\pi v_M t} \left( 1 - \left( \frac{r}{v_M t} \right)^2 \right)^{-1/2} \theta(v_M t - |r|), \quad (10)$$

$$\Delta E_{V2}(r, t) = \frac{2E_0}{\pi v_M t} \left( 1 - \left( \frac{r}{v_M t} \right)^2 \right)^{1/2} \theta(v_M t - |r|), \quad (11)$$

$$\Delta E_D(r, t) = \frac{8E_0}{3\pi v_M t} \left( 1 - \left( \frac{r}{v_M t} \right)^2 \right)^{3/2} \theta(v_M t - |r|). \quad (12)$$

The total energy  $\int dr \Delta E(r, t)$  is  $E_0$  in all three cases. These formulas are shown as dashed lines in Figs. 1 and 3. The continuum model agrees well with an average of nearby values of the local atomic energy  $E(\ell)$  for all of the three pulse types  $E_{\alpha}(\ell)$ . The rms centers of energy of the propagating pulses are then

$$\bar{r}_{\text{continuum}}(t) \equiv \left[ \frac{\int dr r^2 \Delta E(r, t)}{\int dr \Delta E(r, t)} \right]^{1/2}. \quad (13)$$

This is where the result  $d\bar{r}/dt \rightarrow v_M/\sqrt{n}$  (with  $n = 2, 4, 6$ ) came from.

It had been our original guess that when the pulse propagates in a thermal background, the fine structure

in  $E(\ell)$  would disappear and the result would resemble the continuum version  $E(r, t)$ . The computation in Fig. 3 shows that this guess was wrong. The fine structure remains. A proof that this should happen is given in the Supplemental Material<sup>5</sup>.

#### IV. NON-LOCAL BOLTZMANN EQUATION, COLLISIONLESS

The formulas given in Eqs. 10, 11, 12 came from a sensible hypothesis, Eq. 9, which will now be derived from Boltzmann theory. Pulse behavior is fundamentally non-local, and not closely associated with deviation of temperature  $T(r, t)$  from background  $T_0$ . The usual local Boltzmann equation is very successful<sup>6</sup> in describing the bulk thermal conductivity  $\kappa$ , appearing in the Fourier law  $j = -\kappa \nabla T$ , where the temperature gradient  $\nabla T$  is constant in space and time, or varying slowly on the scale of phonon mean free paths  $\ell_Q$  and lifetimes  $\tau_Q$ . Pulse propagation requires an extension of the usual local version. For at least 60 years<sup>7,8</sup> there have been developments of Boltzmann theory aimed at studying systems driven at small distance scales, *i.e.* distances comparable to quasiparticle mean free paths. These developments are not finished.

The Peierls Boltzmann equation (PBE) uses quantum wave/particle duality to describe the system as a gas of phonon particles in a continuous space with coordinate  $r$ , rather than discrete sites  $r_\ell = \ell a$  on a lattice. They can be treated either as classical or quantum particles. A correct treatment of Boltzmann theory with the full scattering operator  $(\partial N_Q / \partial t)_{\text{coll}}$  gives the same low frequency transport properties as a self-consistent treatment by Green-Kubo theory to second order in interactions<sup>9-13</sup>. The fundamental object is  $N_Q(r, t)$ , the occupancy per unit volume  $V$  (where  $V = \text{length } L$  in 1d) of phonon mode  $Q$  at  $(r, t)$ . The spatial sum  $\int dr N_Q(r, t) = N_Q(t)$  is the mode occupancy. The PBE is

$$\frac{\partial N_Q}{\partial t} = -v_Q \frac{\partial N_Q}{\partial r} + \left( \frac{\partial N_Q}{\partial t} \right)_{\text{coll}} + \left( \frac{\partial N_Q}{\partial t} \right)_{\text{ext}}. \quad (14)$$

Local energy is  $E(r, t) = (1/V) \sum_Q \hbar \omega_Q N_Q(r, t)$ . Heat current density is  $j(r, t) = (1/V) \sum_Q \hbar \omega_Q v_Q N_Q(r, t)$ . Local energy is conserved. Summing Eq. 14 over  $Q$  gives

$$\frac{\partial E(r, t)}{\partial t} = -\nabla j(r, t) + \left( \frac{\partial E(r, t)}{\partial t} \right)_{\text{ext}}. \quad (15)$$

This holds because collisions conserve energy locally,  $\sum_Q \hbar \omega_Q (\partial N_Q / \partial t)_{\text{coll}} = 0$ . We will use the quantum version, with an equilibrium Bose-Einstein distribution  $N_Q \rightarrow n_Q(T_0) = [\exp(\hbar \omega_Q / k_B T_0) - 1]^{-1}$ , and take the classical limit  $n_Q(T) = k_B T / \hbar \omega_Q$  when comparing with simulations.

The scattering (or collision) term  $(\partial N_Q / \partial t)_{\text{coll}}$  tries to drive the local distribution to a local thermal distribution. Writing the distribution as  $n_Q(T(r, t)) + \Phi_Q(r, t)$ ,

where  $\Phi_Q$  is the deviation from local equilibrium, and linearizing, Eq. 14 becomes

$$\frac{\partial n_Q}{\partial T} \frac{\partial T}{\partial t} + \frac{\partial \Phi_Q}{\partial t} = -v_Q \left( \frac{\partial n_Q}{\partial T} \frac{\partial T}{\partial r} + \frac{\partial \Phi_Q}{\partial r} \right) - \sum_{Q'} C_{QQ'} \Phi_{Q'} + \left( \frac{\partial N_Q}{\partial t} \right)_{\text{ext}} \quad (16)$$

where  $-C_{QQ'}$  is the linearized scattering operator. The atoms are driven by external manipulation that changes the Newtonian state  $\{u_\ell, v_\ell\}$  to  $\{u_\ell + \Delta u_\ell, v_\ell + \Delta v_\ell\}$  at  $t = 0$ , for  $\ell = 0$  and 1. It changes the phonon amplitudes and phases to give the starting pulse shape. A continuum version of the change must be created by the term  $(\partial N_Q / \partial t)_{\text{ext}}$  in the Boltzmann equation. External driving  $(\partial N_Q / \partial t)_{\text{ext}}$  has only recently appeared in phonon Boltzmann theory<sup>14-17</sup>; its form and significance is still open to discussion. Boltzmann theory does not deal directly with amplitudes  $A_Q$ . These are indirectly included *via* the mode energy  $MA_Q^2 \omega_Q^2 / 2 \rightarrow \hbar \omega_Q (N_Q + 1/2)$ . Coherent phase relations  $\phi_Q$  between different quasiparticles  $Q$  cannot be handled. A choice for the external term  $(\partial N_Q / \partial t)_{\text{ext}}$  driving the distribution function  $N_Q$  away from equilibrium is

$$\left( \frac{\partial N_Q}{\partial t} \right)_{\text{ext}} = \frac{\Delta E_Q^{\text{ext}}}{\hbar \omega_Q} \delta(r) \delta(t). \quad (17)$$

The energy inserted by the pulse into mode  $Q$  is  $\hbar \omega_Q \times \Delta N_Q^{\text{ext}}$ , where  $\Delta N_Q^{\text{ext}} = \int dr \int dt (\partial N_Q(r, t) / \partial t)_{\text{ext}}$ . The total pulse energy given to the system is clearly correct:

$$E_{\text{pulse}}^{\text{Boltzmann}} = \sum_Q \Delta E_Q^{\text{ext}}. \quad (18)$$

Because of linearity and periodic boundary conditions, it is convenient to Fourier transform to  $N_Q(k, \omega)$ ,

$$N_Q(k, \omega) = \frac{1}{L} \int_{-L/2}^{L/2} dr \int_{-\infty}^{\infty} dt N_Q(r, t) e^{-i(kr - \omega t)}. \quad (19)$$

Equation 16 becomes

$$\sum_{Q'} C_{QQ'} \Phi_{Q'} + i(kv_Q - \omega) \Phi_Q = -i(kv_Q - \omega) \frac{\partial n_Q}{\partial T} \Delta T(k, \omega) + \frac{\Delta E_Q^{\text{ext}}}{\hbar \omega_Q}. \quad (20)$$

In the harmonic case, there are no collisions and  $C_{QQ'} = 0$ . The solution in Fourier space is

$$\frac{\partial n_Q}{\partial T} \Delta T(k, \omega) + \Phi_Q(k, \omega) = \frac{\Delta E_Q^{\text{ext}} / \hbar \omega_Q}{i(kv_Q - \omega - i\eta)}. \quad (21)$$

The left hand side is  $\Delta N_Q(k, \omega) = N_Q(k, \omega) - n_Q(T_0)$ . Transforming back to  $(r, t)$ -space,

$$\begin{aligned} \Delta N_Q(r, t) &= \frac{L}{2\pi} \int dk \int \frac{d\omega}{2\pi} \frac{\Delta E_Q^{\text{ext}} / \hbar \omega_Q}{-i(\omega + i\eta - kv_Q)} e^{i(kr - \omega t)} \\ &= \frac{\Delta E_Q^{\text{ext}}}{\hbar \omega_Q} \delta(r - v_Q t) \end{aligned} \quad (22)$$

The local energy density is

$$\bar{E}_{\text{pulse}}(r, t) = \sum_Q \hbar\omega_Q \Delta N_Q(r, t) = \sum_Q \Delta E_Q^{\text{ext}} \delta(r - v_Q t). \quad (23)$$

This agrees exactly with Eq. 9. These results allow confidence in the insertion term added to the Peierls Boltzmann equation. We also learn that, in the continuum description, harmonic pulse shapes (Eqs. 10-12) are independent of  $T$ , because the temperature  $T_0$  in the Boltzmann treatment did not have to be specified. The less obvious result, that harmonic pulse shapes in the atomistic version are also independent of  $T$ , is explained in the Supplemental Material<sup>5</sup>.

## V. MASS DISORDER

Disorder adds an interesting complication to heat conduction in 1-d harmonic crystals<sup>18,19</sup>, namely Anderson localization<sup>20</sup>. In disordered metals of dimension 2 or less, ignoring electron-electron interactions, all single-particle electron eigenstates are localized<sup>21</sup>. At  $T = 0$ , an electron inserted into a localized state cannot propagate. Localization of phonons is similar<sup>22-24</sup>, except that small  $Q$  acoustic phonons have to travel very long distances before localization appears<sup>25</sup>. Reference 26 gives the example of a wave packet propagating on a weakly mass-disordered chain. Ballistic propagation is seen at short distances and times, diffusive propagation at intermediate ones, and Anderson localization at long distances and times. When  $T > 0$ , interactions with phonons allow a localized electron to hop to neighboring localized states, which causes slow diffusion. Anharmonic interactions have a similar effect<sup>27</sup> on localized phonons in insulators. If disorder is not too great, phonon quasiparticles are a realistic model at intermediate times and distances. Ballistic phonons eventually scatter from disorder and evolve toward diffusive at moderate to long distances and times, before localizing. A perturbative treatment of scattering can likely describe the parts before localization sets in.

We now add mass defects to allow deviation from ballistic propagation, by randomly choosing 10% of the atoms, and increasing their masses from  $M = 1$  to  $M^* = 1.5$ . Results at various times for a D pulse are shown in Fig. 4. The lattice is still harmonic, but the Hamiltonian is no longer diagonal in the plane-wave basis, Eq. 2. Before ensemble averaging, the pulse shape varies depending on the locations of the mass defects relative to the point of pulse insertion. The D-pulse shapes of Fig. 4 have been averaged over 100 different random placements of the altered masses.

The pulse shape at  $t = 10\sqrt{M/K}$  is not much altered from pure ballistic behavior. The pulse has propagated only a distance of  $\pm 10$  atoms, and encountered typically only two impurities. As time proceeds, there is increasing deviation from the ballistic pulse shape predicted in Eq. 12, and shown in the red curves. By  $t = 40$ , the

fraction of the energy at distances  $< 10a$  has failed to diminish the way ballistic propagation does. The energy in the intermediate 10 – 30 atoms has diminished more than ballistic propagation does. The crossover toward diffusion is underway. The disorder is weak, so the Anderson localization lengths  $\xi_Q$  are mostly longer than the propagation distance of  $\pm 40$  atoms studied here.

## VI. PURE DIFFUSION

The opposite extreme from ballistic propagation is pure diffusion. The equation for the energy  $\Delta E$  propagating diffusively from a pulse  $P$  is

$$\left( \frac{\partial}{\partial t} - D \frac{d^2}{dr^2} \right) \Delta E(r, t) = P(r, t) = E_0 \delta(r) \delta(t) \quad (24)$$

This follows from energy conservation, Eq. 15, provided there is a local relation  $j = -\kappa dT/dr$  between current  $j(r, t)$  and temperature  $T(r, t)$ . It also uses as the definition of temperature  $\Delta E(r, t) = C\Delta T(r, t)$ . Then the diffusion constant is  $D = \kappa/C$  where  $\kappa$  and  $C$  are bulk thermal conductivity and specific heat. The solution of Eq. 24 is

$$\Delta E_{\text{diff}}(r, t) = \frac{E_0}{\sqrt{4\pi Dt}} e^{-r^2/4Dt} \theta(t), \quad (25)$$

where  $\theta(t)$  is the Heaviside function.

Pure diffusion is inconsistent with a quasiparticle picture of pulse evolution. One argument is that it violates the rule that lattice vibrational energy cannot propagate faster than the speed of sound  $v_M$ . It is not necessarily a large violation. An estimate of the size uses  $\kappa \approx Cv\ell = Cv^2\tau$ . The diffusive exponent  $r^2/4Dt$  is then approximately  $(t/4\tau)(r/v_M t)^2$  (where  $\ell$  and  $\tau$  are rough measures of mean free path and lifetime of phonons). Therefore, when  $t = 4\tau$ , there is some diffusive energy at  $r > v_M t$ , which decays rapidly as  $r/v_M t$  or  $t/4\tau$  increases.

Another argument for the inapplicability of pure diffusion to quasiparticles is that mean free paths of small  $Q$  acoustic phonons typically diverge as a power,  $\ell_Q \propto 1/Q^p$ , causing  $D$  to diverge. This is a correct result, not an error of perturbation theory. A formula for  $D = \kappa/C$  is found from the standard RTA solution of Boltzmann theory for  $\kappa$  in the bulk limit,

$$D = \frac{\sum_Q C_Q v_Q^2 \tau_Q}{\sum_Q C_Q} \rightarrow \frac{1}{N} \sum_Q v_Q^2 \tau_Q. \quad (26)$$

The second form is the classical limit where  $C_Q = \hbar\omega_Q dn_Q/dT \rightarrow k_B$ . When  $1/\tau_Q$  arises from mass disorder, the small  $Q$  scattering rate  $1/\tau_Q$  in  $d = 1$  goes as  $(Q^2)^{18,28-30}$ , shown explicitly in appendix A. The divergence is not limited to one dimension. Small  $Q$  scattering from mass defects is closely analogous to Rayleigh scattering of light from density fluctuations. In 3d, both light

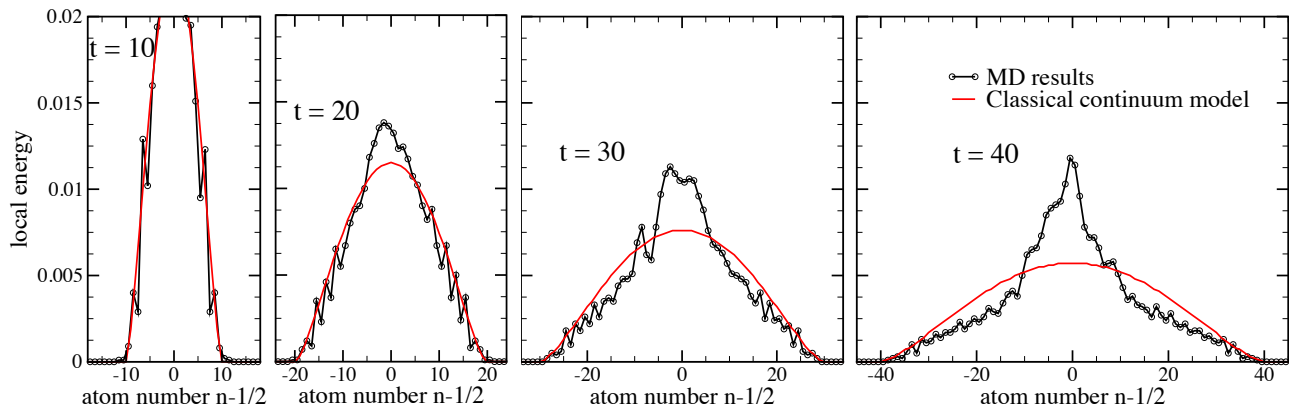


FIG. 4. Total energy profile  $E_a(\ell)$  of a  $\mathbf{D}$ -pulse at  $T = 0$ , after spreading in the lattice with 10% of the masses increased by 1.5. The profiles are averaged over 100 random realizations of mass disorder. Time is in units  $\sqrt{M/K}$ . The red curves are the ballistic prediction of Eq. 12. The value of  $E_0$  has been rescaled from 1 to 0.27, corresponding to  $u_0 = 0.3$ , which is the value chosen for this and subsequent computations.

and phonon scattering have  $Q^4$  dependences at small  $Q$ . The  $Q$ -sum needed to compute  $D$  or  $\kappa$  diverges as  $1/Q^2$  in both  $d = 1$  and  $d = 3$ , unless another scattering process adds a term to  $1/\tau_Q$  that blocks the divergence. When  $T$  is small enough that mean free paths  $\ell_Q = v_Q\tau_Q$  reach sample dimensions  $L$ , the zero denominator from the diverging defect term becomes non-zero due to boundary scattering  $L = v_Q\tau_{\text{boundary}}$ . Glassbrenner and Slack analyze experiments which illustrate this<sup>31</sup>. It is seen in clean but isotopically disordered crystals<sup>32,33</sup>. Eqn. 26 can be replaced by

$$D = \sum_Q v_Q^2 [(1/\tau_Q)_{\text{disorder}} + |v_Q|/L]^{-1}. \quad (27)$$

The sum now converges, diverging for large  $L$  as  $D \propto \sqrt{L}$  in  $d = 1$ . The  $\sqrt{L}$  scaling of  $\kappa$  in  $d=1$  was noticed earlier<sup>18,34</sup>. The resulting  $D$  is plotted *versus*  $L/a$  in Fig. 5. Our Newtonian simulation on a loop of 200 atoms has no boundary scattering because of periodic boundary conditions. If we had used instead rough boundaries, then  $L$  in Eq. 27 would be  $100a$ , resulting in  $D = 35\omega_M a^2/2$  (see Appendix A).

In spite of the inapplicability of Eq. 25, it is interesting to compare it to the numerical results. Figure 6 compares the simulation result of the disordered  $\mathbf{D}$ -pulse at  $t = 40$  (the last graph of Fig. 4) with the formulas for pure ballistic and pure diffusive propagation. For the majority of atoms (all but atoms 10-14) the computed pulse energy is closer to the green curve illustrating pure diffusion (with  $D = 1.8$ ) than to the red curve of pure ballistic behavior. However, the agreement with pure diffusion is poor, and more important, the choice  $D = 1.8$  was chosen to be close to the simulation, but is totally unrealistic, corresponding to a nanoscale sample with boundaries at  $\approx \pm 3a$ , as seen from Fig. 5.

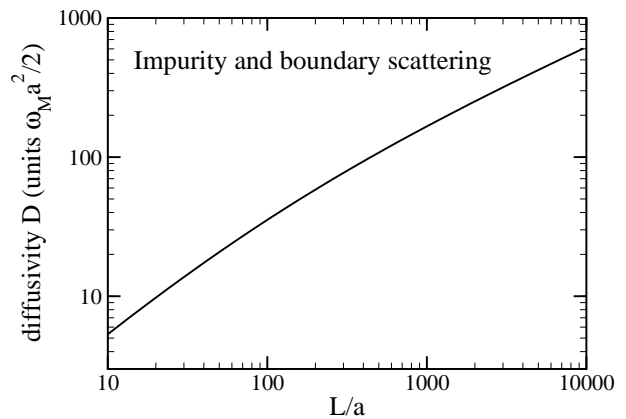


FIG. 5. The diffusivity in bulk RTA theory, from Eq. 27 and A4, using Eq. 28 for the disorder scattering, with the dimensionless strength  $\epsilon = 1/90$ . The diffusivity diverges as  $\sqrt{L/\epsilon}$  as  $L \rightarrow \infty$ .

## VII. BOLTZMANN THEORY WITH MASS DISORDER

How does non-local Boltzmann theory treat pulse shape evolution as altered by disorder? Here we answer this question within the relaxation time approximation (RTA), and find that the results have the correct trend but do not agree closely with simulations. The collision operator  $C_{QQ'}$  in Eq. 20 is replaced in RTA by  $1/\tau_Q\delta_{QQ'}$ , where  $1/\tau_Q$  is the diagonal element,  $C_{QQ}$ ,

$$1/\tau_Q = \epsilon\omega_M \frac{\sin^2(Qa/2)}{\cos(Qa/2)}. \quad (28)$$

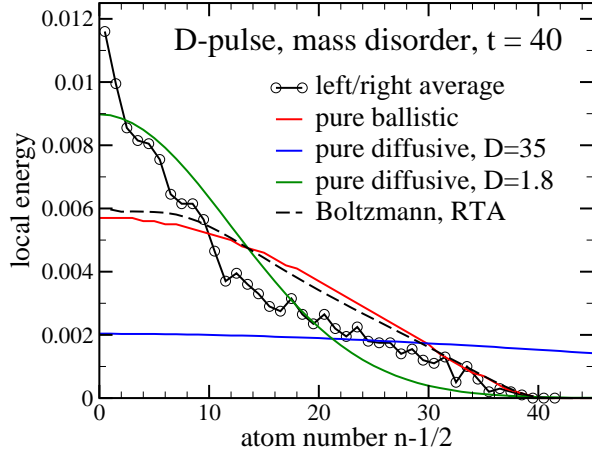


FIG. 6. The same  $t = 40$  pulse energy profile  $E_a(\ell)$  as in Fig. 4, but showing only  $x > 0$  and averaging the left and right propagating portions. The red curve is the ballistic prediction of Eq. 12, and the blue curve is the diffusive prediction of Eq. 25, with diffusion constant  $D = 35a^2\omega_M/2$  as explained in the text. The green curve is the same, except  $D = 1.8a^2\omega_M/2$  is used to make diffusion appear closer to the computed pulse profile. The dashed curve is the Boltzmann prediction (with no boundary scattering) using version (1) of RTA, shown in Eq. 30 and explained in section VII. All “theoretical” curves are scaled to  $E_0 = 0.27$  to agree with the numerical simulation.

This is derived in appendix A, Eq. A3. The RTA solution is a modified version of Eq. 21,

$$\Phi_Q(k, \omega) = \frac{-i(kv_Q - \omega) \frac{\partial n_Q}{\partial T} \Delta T(k, \omega) + \Delta E_Q^{\text{ext}} / \hbar\omega_Q}{1/\tau_Q + i(kv_Q - \omega)}. \quad (29)$$

This gives  $N$  equations (one for each mode  $Q$ ), for the  $N$  unknown functions  $\Phi_Q(k, \omega)$ . There is an additional unknown, the local temperature shift  $\Delta T(k, \omega)$ . An extra equation, to supplement Eq. 29, is needed.

The requirement of energy conservation says that  $\sum_Q \hbar\omega_Q (d\Phi_Q/dt)_{\text{coll}} = 0$ . The correct scattering operator satisfies this automatically, but the RTA version,  $(dE/dt)_{\text{coll,RTA}} = -\sum_Q \hbar\omega_Q \Phi_Q / \tau_Q = 0$ , is **not** automatically satisfied. Forcing  $\Phi_Q$  to satisfy this equation as well as the linearized PBE is one way to obtain the extra equation needed to determine  $\Delta T(k, \omega)$  and  $\Delta T(r, t)$ . This definition of temperature is not a normal one. A possible alternative is to define temperature in terms of the local energy,  $E(r, t) = \sum_Q \hbar\omega_Q n_Q(T(r, t))$  or  $E(k, \omega) = \sum_Q \hbar\omega_Q (dn_Q/dT) \Delta T(k, \omega)$ . This is the definition of  $\Delta T(k, \omega)$  used in the full Boltzmann equation with the correct scattering operator. It requires the deviation  $\Phi_Q(r, t)$  to have no net energy. This definition of temperature is quite normal - it is sensible in a quasiparticle theory, although perhaps not demanded by nonequilibrium thermodynamics.

The two possible versions of the extra equation are

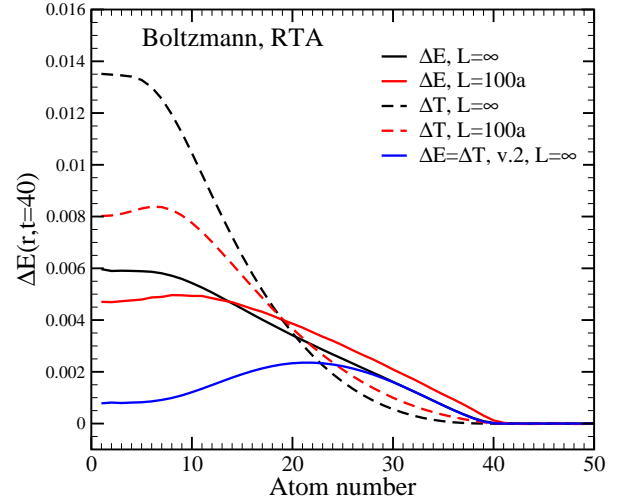


FIG. 7. RTA predictions for the total energy profile  $E_a(\ell)$  of a  $\mathbf{D}$ -pulse at  $t = 40$  and  $T = 0$ , after spreading in the lattice with 10% of the masses increased by 1.5. The input energy  $E_0$  is set to 0.27, for comparison with numerical results. The red and black curves use version (1) of Eq. 30, and the blue curve uses version (2). The total energy (solid curves) correctly agrees with  $E_0$  in version (1), but in version (2), is smaller by a factor 0.415. In version (1), the thermal energy is (incorrectly, we believe) larger than  $E_0$  by a factor 1.58.

then

$$(1) \sum_Q \frac{\hbar\omega_Q \Phi_{Q,\text{RTA}}}{\tau_Q} = 0; \text{ or } (2) \sum_Q \hbar\omega_Q \Phi_{Q,\text{RTA}} = 0. \quad (30)$$

We find that version (1) gives a more realistic answer, in agreement with previous numerical<sup>35</sup> and theoretical<sup>15–17</sup> work.

The pulse energy predicted by version (1) is shown in Fig. 6. It deviates less from ballistic than does the simulation, but in the correct direction. Energy profiles predicted by both versions of the RTA Boltzmann theory are in Fig. 7 for the  $\mathbf{D}$  pulse at  $t = 40$ . Details of the computational procedure are given in appendix B and in the Supplemental Material<sup>5</sup>. Version (1) of RTA theory correctly keeps the total pulse energy equal to  $E_0$  as  $t$  increases, while version (2) does not. Version (2) has another weakness, namely the predicted shape of the evolving pulse in Fig. 7 is very different from the simulated results in Fig. 6, unlike version (1) where the Boltzmann-RTA pulse shape is sensible. However, version (1) has a temperature profile  $\Delta T(r, t)$  in Fig. 7 that differs from  $\Delta E(r, t)$  without physical justification, unlike version (2) which correctly equates  $k_B T(r, t)$  and  $\Delta E(r, t)$ .

Figure 8 shows version (1) results for long times to illustrate a slow approach toward something related to, but not closely agreeing with, pure diffusion, Eq. 25. The RTA diffusivity  $D = 1.8$  used in the dashed curve of Fig. 8 uses an unrealistically small sample size,  $\approx 3a$ , as mentioned already. These results confirm the arguments

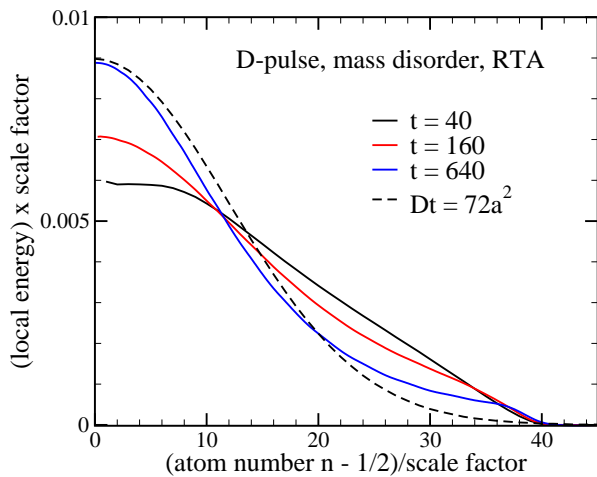


FIG. 8. Boltzmann results using RTA, with impurity but no boundary scattering, at three times,  $t = 40, 160,$  and  $640$ . Time is in units  $2/\omega_M = 1$ . The scale factors 1, 4, and 16 are used to keep the correct area ( $E_0 = 0.27$ ) while scaling the horizontal distance  $v_M t$  to 40 to make the results fit on a single graph. The dashed line is pure diffusion  $\propto \exp(-x^2/4Dt)$  (Eq. 25) at  $t = 40$ , with the same arbitrary diffusivity  $D = 1.8\omega_M a^2/2$  used in Fig. 6, chosen just to illustrate pure diffusion.

in Sec. VI that pure diffusion disagrees with quasiparticle theories.

Why do the Boltzmann-RTA results not agree well with the numerical pulse shapes? The reason could be a mixture of two problems: (1) inadequacy of second order Fermi golden rule, related to incipient Anderson localization; and (2) use of RTA instead of correct local energy-conserving scattering.

### VIII. ANHARMONIC

The famous work of Fermi, Pasta, Ulam (FPU) and Tsingou (FPUT)<sup>36</sup> found unexpected anomalies in the opposite limit of our pulse propagation, namely the zero temperature behavior of the lowest harmonic normal mode of the fixed-end chain, when propagated with one or the other of two anharmonic nearest neighbor couplings,

$$\mathcal{H}'_3 = \frac{V_3}{3} \sum_{\ell} (r_{\ell+1} - r_{\ell})^3 \quad (V_3 = \alpha K, \text{ the } \alpha - \text{model}); \quad (31)$$

$$\mathcal{H}'_4 = \frac{V_4}{4} \sum_{\ell} (r_{\ell+1} - r_{\ell})^4 \quad (V_4 = \beta K, \text{ the } \beta - \text{model}). \quad (32)$$

Heat conduction in weakly anharmonic linear lattices has been studied<sup>37</sup> and reviewed<sup>38</sup>. Recent work<sup>39–41</sup> seems to confirm (at least qualitatively) that perturbation theory works in the regime studied here. If so, the

perturbative picture says that mean free paths will diminish as  $T$  increases<sup>42,43</sup>. A crossover to diffusive behavior, which FPU indicates might not happen at  $T = 0$ , may well happen at  $T > 0$ , at rates that increase as  $T$  increases.

We have looked at  $T = 0$  anharmonic pulse propagation, using both third-order ( $V_3$ , also known as “FPU- $\alpha$ ”) and fourth-order ( $V_4$ , also known as “FPU- $\beta$ ”) anharmonicity. The coefficients  $\alpha$  and  $\beta$  in Eqs. 31 and 32 were set to 1. Local energy  $E(\ell, t)$  is defined as in Eq. 3: the total (harmonic and anharmonic) potential energy of a spring is assigned half to each neighboring atom. The results are in Fig. 9. The initial pulse ( $u_{0,1} = \pm 0.3$ ) is the same as in previous computations, except the total energy is no longer  $0.27E_0$  as in previous computations, because there is additional anharmonic energy,  $-27\%$  in  $V_3$  and  $+12\%$  in  $V_4$ . The initial pulse has the same harmonic amplitudes  $A_Q$  and phases  $\phi_Q$  as previously, but anharmonic terms alter these fairly quickly. As the pulse spreads and  $\Delta E(\ell, t)$  spreads out, anharmonic forces diminish. Amplitudes and phases evolve less, becoming more stable. As  $t$  increases, local energy propagation from  $(x, t)$  reverts more closely to ballistic. This is especially noticeable in the  $V_3$  case, where atoms 10 – 16 seem little affected by anharmonic effects. The  $V_3$  case might be especially difficult to analyze perturbatively, because in lowest order and 1d, anharmonic decay is essentially kinematically forbidden, requiring higher order effects to change  $A_Q$  and  $\phi_Q$ . It would be interesting to study the anharmonic pulse at finite  $T$  where anharmonic effects do not disappear as the pulse propagates.

### IX. CONCLUSIONS

Time evolution of pulse energy gives useful pictures and insights into non-local phonon transport. The main conclusions are: (1) Different forms of pulse insertions give interestingly diverse pulse energy shapes. (2) Atomistic local energy  $E(\ell, t)$  is not uniquely defined and has surprisingly different details when different sensible definitions are used. (3) A continuum picture works well and enables simple formulas for ballistic propagation. (4) A non-local version of Boltzmann theory for the collisionless phonon gas is very successful, and the phonon insertion term  $(\partial N_Q/\partial t)_{\text{ext}}$  has an unambiguous form. (5) Mildly disordered harmonic systems have interesting pulse evolution, but are not well explained by non-local Boltzmann theory in relaxation time approximation (RTA). Ambiguity about temperature definition in RTA is a difficulty; previous ideas are confirmed. (6) Pure diffusion does not work at the local level, when phonon quasiparticles are good approximations, even after long pulse evolution times. (7) The pulse evolution of 1d anharmonic chains at  $T > 0$  deserves further study.

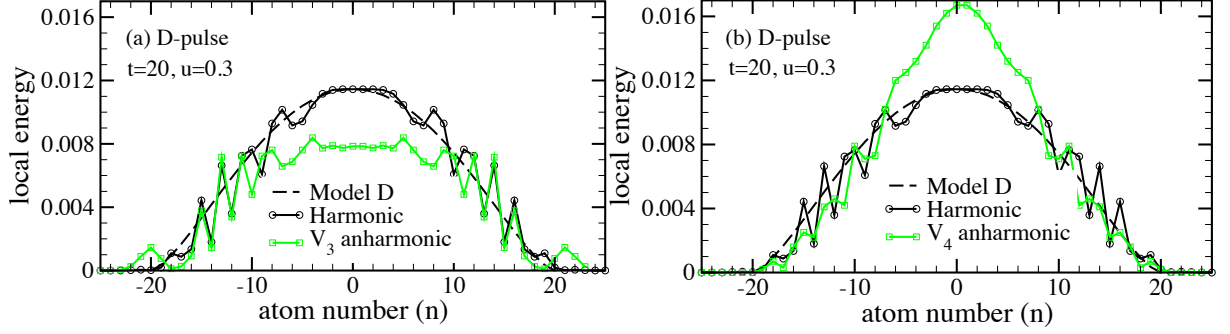


FIG. 9. Displacement (**D**) pulse at time  $t = 20$  after insertion at  $T = 0$  and  $t = 0$ . The harmonic ( $K_2$ ) force constant is 1. (a) has  $V_3 = 1$  and  $V_4 = 0$ ; (b) has  $V_3 = 0$  and  $V_4 = 1$ . The pure harmonic result ( $V_3 = V_4 = 0$ ) is shown for comparison in both panels. To see the effect of anharmonicity, initial pulse amplitudes on atoms 0 and 1 were given large values, 0.3 and -0.3, respectively. The initial anharmonic energy in (a) is  $-0.27 \times$  the initial harmonic energy ( $0.27E_0$ ), and in (b)  $+0.12 \times$  the initial harmonic energy ( $0.27E_0$ ).

## X. ACKNOWLEDGEMENTS

We are grateful to the Stony Brook Institute for Advanced Computational Science for use of their computer cluster.

### Appendix A: Phonon relaxation from mass disorder

The Fermi golden rule for phonon decay by defects is  $1/\tau_Q = (2\pi/\hbar) \sum_{Q'} |V_{QQ'}|^2 \delta(\hbar\omega_Q - \hbar\omega_{Q'})$ . When the interaction  $V_{QQ'}$  arises from mass disorder, the decay rate is

$$\left(\frac{1}{\tau_Q}\right)_{\text{imp}} = \frac{\pi}{2\hbar} \frac{N_i}{N} \left(\frac{\Delta M}{M^*}\right)^2 (\hbar\omega_Q)^2 \mathcal{D}(\omega_Q), \quad (\text{A1})$$

where  $\Delta M = M^* - M$  is the mass difference between impurities ( $M^*$ ) and pure ( $M$ ) masses, and  $N_i/N$  is the fraction of impurities. The density of vibrational states of the ordered harmonic chain is

$$\mathcal{D}(\omega) = \frac{1}{\hbar N} \sum_Q \delta(\omega - \omega_Q) = \frac{2}{\pi\hbar} \frac{1}{(\omega_M^2 - \omega^2)^{1/2}}. \quad (\text{A2})$$

Then the decay rate is

$$\frac{1}{\tau_Q} = \epsilon \frac{\omega_Q^2}{(\omega_M^2 - \omega_Q^2)^{1/2}}, \quad \text{where } \epsilon = \frac{N_i}{N} \left(\frac{\Delta M}{M^*}\right)^2, \quad (\text{A3})$$

and  $\epsilon = 1/90$  in our simulations.

The formula 27 for boundary-limited diffusivity can be written as

$$D(L) = \frac{\omega_M a^2}{2} \frac{s}{\pi\epsilon} \int_0^{\pi/2} dx \frac{\cos^3 x}{\cos^2 x + s \sin^2 x}, \quad (\text{A4})$$

where  $s = 2L\epsilon/a$  and  $\omega_M a^2/2 = 1$  is the unit of diffusivity. At large  $s$ , the diffusivity scales as  $\sqrt{s}/\epsilon \propto \sqrt{L/\epsilon}$ .

### Appendix B: Solution of Boltzmann equation in RTA

Using Eq. 29 and version (1) of Eq. 30, the equation for  $\Delta T$  is

$$k_B \Delta T_{(1)}(k, \omega) = \frac{A(k, \omega)}{B(k, \omega)}, \quad (\text{B1})$$

where

$$A(k, \omega) = \frac{1}{N} \sum_Q \frac{\Delta E_Q^{\text{ext}}/\tau_Q}{1/\tau_Q - i(\omega - kv_Q)}, \quad (\text{B2})$$

$$B(k, \omega) = \frac{1}{N} \sum_Q \frac{1}{\tau_Q} \frac{-i(\omega - kv_Q) \left[ \frac{\hbar\omega_Q}{k_B} \frac{\partial n_Q}{\partial T} \right]}{1/\tau_Q - i(\omega - kv_Q)}. \quad (\text{B3})$$

Once  $\Delta T_{(1)}(k, \omega)$  is computed, the corresponding local energy  $\Delta E_{(1)}(k, \omega)$  can be found and Fourier transformed to get  $\Delta E_{(1)}(r, t)$ ,

$$\begin{aligned} \Delta E_{(1)}(k, \omega) &\equiv \sum_Q \hbar\omega_Q [N_Q - n_Q(T_0)] \\ &= C(k, \omega) k_B \Delta T_{(1)}(k, \omega) + D(k, \omega), \end{aligned} \quad (\text{B4})$$

where

$$C(k, \omega) = \frac{1}{N} \sum_Q \frac{1/\tau_Q \left[ \frac{\hbar\omega_Q}{k_B} \frac{\partial n_Q}{\partial T} \right]}{1/\tau_Q - i(\omega - kv_Q)}, \quad (\text{B5})$$

$$D(k, \omega) = \frac{1}{N} \sum_Q \frac{\Delta E_Q^{\text{ext}}}{1/\tau_Q - i(\omega - kv_Q)}. \quad (\text{B6})$$

The factor in square brackets ( $[ ]$ ) in Eqs. B3 and B5 (and later in Eq. B9) becomes 1 in the classical limit, which is needed for comparison with the numerical pulse spreading.

To implement version (2), use the simpler condition

$$\Delta E_{(2)}(k, \omega) = k_B \Delta T_{(2)}(k, \omega). \quad (\text{B7})$$

Using Eq. 29 and version (2) of Eq. 30, the equation for  $\Delta E$  is

$$\Delta E_{(2)}(k, \omega) = k_B \Delta T_{(2)}(k, \omega) = \frac{D(k, \omega)}{F(k, \omega)}, \quad (\text{B8})$$

where, except for omission of factors of  $1/\tau_Q$  in the numerator,  $D(k, \omega)$  is the same as  $A(k, \omega)$  and  $F(k, \omega)$  is the same as  $B(k, \omega)$ . To be explicit,

$$F(k, \omega) = \frac{1}{N} \sum_Q \frac{-i(\omega - kv_Q) \left[ \frac{\hbar \omega_Q}{k_B} \frac{\partial n_Q}{\partial T} \right]}{1/\tau_Q - i(\omega - kv_Q)}. \quad (\text{B9})$$

Details of the numerical calculations, especially the difficult Fourier transforms needed to get pulse shapes in  $(x, t)$ -space, are in the Supplemental Materials<sup>5</sup>.

- 
- \* philip.allen@stonybrook.edu
- <sup>1</sup> Sha Liu, P. Hänggi, Nianbei Li, Jie Ren, and Baowen Li, “Anomalous heat diffusion,” *Phys. Rev. Lett.* **112**, 040601 (2014).
  - <sup>2</sup> Chengyun Hua and Lucas Lindsay, “Space-time dependent thermal conductivity in nonlocal thermal transport,” *Phys. Rev. B* **102**, 104310 (2020).
  - <sup>3</sup> A. Marcolongo, P. Umari, and S. Baroni, “Microscopic theory and quantum simulation of atomic heat transport,” *Nature Physics* **12**, 80 – 84 (2016).
  - <sup>4</sup> L. Ercole, A. Marcolongo, P. Umari, and S. Baroni, “Gauge invariance of thermal transport coefficients,” *J. Low Temp. Phys.* **185**, 79–86 (2016).
  - <sup>5</sup> P. B. Allen and N. A. Nghiem, “Supplemental material for nonlocal phonon heat transport seen in 1-d pulses,” .
  - <sup>6</sup> L. Lindsay, A. Katre, A. Cepellotti, and N. Mingo, “Perspective on ab initio phonon thermal transport,” *J. Appl. Phys.* **126**, 050902 (2019).
  - <sup>7</sup> S. Simons, “The Boltzmann equation for a bounded medium I. General theory,” *Phil. Trans. Roy. Soc. London, Series A, Math. Phys. Sci.* **253**, 137–184 (1960).
  - <sup>8</sup> R. A. Guyer and J. A. Krumhansl, “Solution of the linearized phonon Boltzmann equation,” *Phys. Rev.* **148**, 766–778 (1966).
  - <sup>9</sup> C. Horie and J. A. Krumhansl, “Boltzmann equation in a phonon system,” *Phys. Rev.* **136**, A1397–A1407 (1964).
  - <sup>10</sup> W. Götze and K. H. Michel, “Two-fluid transport equations for lattices,” *Phys. Rev.* **157**, 738–743 (1967).
  - <sup>11</sup> R. Klein and R. K. Wehner, “Derivation of transport equations for anharmonic lattices,” *Physik der kondensierten Materie* **10**, 1–20 (1969).
  - <sup>12</sup> J. Ranninger, “Thermal conductivity in nonconducting crystals,” *Annals of Physics* **45**, 452–478 (1967).
  - <sup>13</sup> H. Spohn, “The phonon Boltzmann equation, properties and link to weakly anharmonic lattice dynamics,” *J. Stat. Phys.* **124**, 1041 – 1104 (2006).
  - <sup>14</sup> Chengyun Hua and A. J. Minnich, “Analytical Green’s function of the multidimensional frequency-dependent phonon Boltzmann equation,” *Phys. Rev. B* **90**, 214306 (2014).
  - <sup>15</sup> B. Vermeersch and A. Shakouri, “Nonlocality in microscale heat conduction,” *ArXiv e-prints* (2014), arXiv:1412.6555v2.
  - <sup>16</sup> B. Vermeersch, J. Carrete, N. Mingo, and A. Shakouri, “Superdiffusive heat conduction in semiconductor alloys. I. Theoretical foundations,” *Phys. Rev. B* **91**, 085202 (2015).
  - <sup>17</sup> Chengyun Hua and A. J. Minnich, “Semi-analytical solution to the frequency-dependent Boltzmann transport equation for cross-plane heat conduction in thin films,” *J. Appl. Phys.* **117**, 175306 (2015).
  - <sup>18</sup> H. Matsuda and K. Ishii, “Localization of Normal Modes and Energy Transport in the Disordered Harmonic Chain,” *Prog. Theor. Phys. Supplement* **45**, 56–86 (1970).
  - <sup>19</sup> W. M. Visscher, “Localization of Normal Modes and Energy Transport in the Disordered Harmonic Chain\*,” *Prog. Theor. Phys.* **46**, 729–736 (1971).
  - <sup>20</sup> P. W. Anderson, “Absence of diffusion in certain random lattices,” *Phys. Rev.* **109**, 1492–1505 (1958).
  - <sup>21</sup> E. Abrahams, P. W. Anderson, D. C. Licciardello, and T. V. Ramakrishnan, “Scaling theory of localization: Absence of quantum diffusion in two dimensions,” *Phys. Rev. Lett.* **42**, 673–676 (1979).
  - <sup>22</sup> Ping Sheng, *Introduction to Wave Scattering, Localization and Mesoscopic Phenomena, 2<sup>nd</sup> edition* (Springer, Berlin, 2005).
  - <sup>23</sup> T. R. Kirkpatrick, “Localization of acoustic waves,” *Phys. Rev. B* **31**, 5746–5755 (1985).
  - <sup>24</sup> M. N. Luckyanova, J. Mendoza, H. Lu, B. Song, S. Huang, J. Zhou, M. Li, Y. Dong, H. Zhou, J. Garlow, L. Wu, B. J. Kirby, A. J. Grutter, A. A. Puzosky, Y. Zhu, M. S. Dresselhaus, A. Gossard, and G. Chen, “Phonon localization in heat conduction,” *Science Advances* **4**, 9460:1–10 (2018).
  - <sup>25</sup> Stefano Lepri, Roberto Livi, and Antonio Politi, “Thermal conduction in classical low-dimensional lattices,” *Physics Reports* **377**, 1–80 (2003).
  - <sup>26</sup> P. B. Allen and J. Kelner, “Evolution of a vibrational wave packet on a disordered chain,” *Am. J. Phys.* **66**, 497–506 (1998).
  - <sup>27</sup> J. Fabian and P. B. Allen, “Anharmonic decay of vibrational states in amorphous silicon,” *Phys. Rev. Lett.* **77**, 3839–3842 (1996).
  - <sup>28</sup> R. J. Rubin and W. L. Greer, “Abnormal lattice thermal conductivity of a one-dimensional, harmonic, isotopically disordered crystal,” *J. Math. Phys.* **12**, 1686–1701 (1971).
  - <sup>29</sup> T. Verheggen, “Transmission coefficient and heat conduction of a harmonic chain with random masses: Asymptotic estimates on products of random matrices,” *Commun. Math. Phys.* **68**, 69–82 (1979).
  - <sup>30</sup> A. Dhar, “Heat transport in low-dimensional systems,” *Advances in Physics* **57**, 457–537 (2008).
  - <sup>31</sup> C. J. Glassbrenner and G. A. Slack, “Thermal conductivity of silicon and germanium from 3K to the melting point,” *Phys. Rev.* **134**, A1058–A1069 (1964).
  - <sup>32</sup> P. D. Thacher, “Effect of boundaries and isotopes on the thermal conductivity of LiF,” *Phys. Rev.* **156**, 975–988 (1967).

- <sup>33</sup> M. Asen-Palmer, K. Bartkowski, E. Gmelin, M. Cardona, A. P. Zhernov, A. V. Inyushkin, A. Taldenkov, V. I. Ozhogin, K. M. Itoh, and E. E. Haller, “Thermal conductivity of germanium crystals with different isotopic compositions,” *Phys. Rev. B* **56**, 9431–9447 (1997).
- <sup>34</sup> J. B. Keller, G. C. Papanicolaou, and J. Weilenmann, “Heat conduction in a one-dimensional random medium,” *Commun. Pure Appl. Math.* **31**, 583–592 (1978).
- <sup>35</sup> P. B. Allen and V. Perebeinos, “Temperature in a Peierls-Boltzmann treatment of nonlocal phonon heat transport,” *Phys. Rev. B* **98**, 085427 (2018).
- <sup>36</sup> E. Fermi, J. Pasta, and S. Ulam, “Studies of the nonlinear problems, I,” Los Alamos Report LA-1940 (1955), later published in *Collected Papers of Enrico Fermi*, ed. E. Segre, Vol. II (University of Chicago Press, 1965) p.978; also reprinted in *Nonlinear Wave Motion*, ed. A. C. Newell, Lecture Notes in Applied Mathematics, Vol. 15 (AMS, Providence, RI, 1974), also in *Many-Body Problems*, ed. D. C. Mattis (World Scientific, Singapore, 1993).
- <sup>37</sup> S. Lepri, “Memory effects and heat transport in one-dimensional insulators,” *Eur. Phys. J. B* **18**, 441–446 (2000).
- <sup>38</sup> J. Lukkarinen, “Kinetic theory of phonons in weakly anharmonic particle chains,” in *Thermal Transport in Low Dimensions: From Statistical Physics to Nanoscale Heat Transfer*, edited by S. Lepri (Springer, Cham, Switzerland, 2016) pp. 159–214.
- <sup>39</sup> G. Dematteis, L. Rondoni, D. Proment, F. De Vita, and M. Onorato, “Coexistence of ballistic and Fourier regimes in the  $\beta$  Fermi-Pasta-Ulam-Tsingou lattice,” *Phys. Rev. Lett.* **125**, 024101 (2020).
- <sup>40</sup> Stefano Lepri, Roberto Livi, and Antonio Politi, “Too close to integrable: Crossover from normal to anomalous heat diffusion,” *Phys. Rev. Lett.* **125**, 040604 (2020).
- <sup>41</sup> Jianjin Wang, Sergey V. Dmitriev, and Daxing Xiong, “Thermal transport in long-range interacting Fermi-Pasta-Ulam chains,” *Phys. Rev. Research* **2**, 013179 (2020).
- <sup>42</sup> A. A. Maradudin, “On the lifetime of phonons in one-dimensional crystals,” *Phys. Lett.* **2**, 298–300 (1962).
- <sup>43</sup> J. Conway, “Decay rate of phonons in a 1-dimensional crystal,” *Phys. Lett.* **17**, 23–24 (1965).

## Supplemental Material for

### Nonlocal Phonon Heat Transport Seen in 1-d Pulses

Philip B. Allen\* and Nhat A. Nghiem

*Department of Physics and Astronomy, Stony Brook University, Stony Brook, NY 11794-3800, USA*

(Dated: September 20, 2022)

In the first section, some mathematics of disordered harmonic systems is used to show that thermal disorder in a harmonic chain will not erase the details of atomistic pulse energy, as shown in Fig. 3 of the full text. In the second section, formulas are given for the five functions used to compute the pulse energy in  $(k, \omega)$ -space, and the  $Q$ -integration is described. In the last section, some details of the numerical Fourier transform to  $(x, t)$ -space are given. When equations from the full text are cited, they are indicated as, for example, Eq. T6.

#### I. CLASSICAL HARMONIC DISORDERED LATTICE

The most general harmonic linear chain is described by

$$\mathcal{H} = \frac{1}{2} \sum_{\ell} \dot{w}_{\ell}^2 + \frac{1}{2} \sum_{\ell} \Omega_{\ell\ell'} w_{\ell} w_{\ell'}, \quad (1)$$

where  $w_{\ell} = \sqrt{M_{\ell}} u_{\ell}$  and  $\Omega_{\ell\ell'} = K_{\ell, \ell'} / \sqrt{M_{\ell} M_{\ell'}}$ . The spring constant  $K_{\ell\ell'}$  is  $\partial^2 U_{\text{PE}} / \partial u_{\ell} \partial u_{\ell'}$ . Vibrational eigenstates  $|\mu\rangle$  are solutions of  $\hat{\Omega}|\mu\rangle = \omega_{\mu}^2 |\mu\rangle$ . The general solution of Newton's laws is described by  $N$  amplitudes  $A_{\mu}$  and phases  $\phi_{\mu}$ ,

$$w_{\ell}(t) = \frac{1}{\sqrt{N}} \sum_{\mu} A_{\mu} \mu_{\ell} \cos(\omega_{\mu} t - \phi_{\mu}), \quad \text{where } \mu_{\ell} = \langle \ell | \mu \rangle. \quad (2)$$

The normal mode coordinates  $\mu_{\ell} = \langle \ell | \mu \rangle$  are defined to be real numbers. For ordered chains of atoms, the simpler convention is to use complex numbers  $\langle \ell | Q \rangle = \exp(iQ\ell a) / \sqrt{N}$ , but real numbers (cosines and sines) also work.

The normal modes are orthonormal,

$$\langle \mu | \mu' \rangle = \sum_{\ell} \langle \mu | \ell \rangle \langle \ell | \mu' \rangle = \frac{1}{N} \sum_{\ell} \mu_{\ell} \mu'_{\ell} = \delta_{\mu\mu'}. \quad (3)$$

From this it is easy to show that

$$\begin{aligned} \text{KE} &= \frac{1}{2} \sum_{\mu} \omega_{\mu}^2 A_{\mu}^2 \sin^2(\omega_{\mu} t - \phi_{\mu}), \\ \text{PE} &= \frac{1}{2} \sum_{\mu} \omega_{\mu}^2 A_{\mu}^2 \cos^2(\omega_{\mu} t - \phi_{\mu}), \end{aligned} \quad (4)$$

and therefore the total energy is

$$E_{\text{tot}} = \sum_{\mu} E_{\mu}, \quad \text{where } E_{\mu} = \frac{1}{2} \omega_{\mu}^2 A_{\mu}^2. \quad (5)$$

This is the generalization to lattices (whether ordered or disordered), of Eq. T8 for ordered lattices. It is also easy to derive the formula

$$A_{\mu} e^{i(\phi_{\mu} - \omega_{\mu} t)} = \frac{1}{\sqrt{N}} \sum_{\ell} \sqrt{M_{\ell}} \left( u_{\ell}(t) + i \frac{v_{\ell}(t)}{\omega_{\mu}} \right) \mu_{\ell}. \quad (6)$$

This is the generalization of Eq. T6. From this formula, one can extract the amplitude  $A_{\mu}$  and phase  $\phi_{\mu}$  of any normal mode  $\mu$  if the positions  $u_{\ell}$  and velocities  $v_{\ell}$  are known at any particular time  $t$ . For example, consider a V1 pulse inserted at zero temperature. Using Eq. 6 at  $t = 0$ , the modal energy is

$$\begin{aligned} E_{\mu}^{\text{V1}, T=0} &= \frac{1}{2} \omega_{\mu}^2 A_{\mu}^2 = \frac{M_{\ell=0}}{2N} \Delta v_{\ell=0}^2 \mu_{\ell=0}^2 \\ &= E_{\text{pulse}}^{\text{V1}} \frac{\langle \ell=0 | \mu \rangle \langle \mu | \ell=0 \rangle}{N} \\ E_{\text{pulse}}^{\text{V1}} &= \sum_{\mu} E_{\mu}^{\text{V1}, T=0} = \frac{M_0 \Delta v_0^2}{2}. \end{aligned} \quad (7)$$

From these results, we can make a tedious proof (for the V1 case) that when temperature is not zero, the ensemble average energy in each mode  $\mu$  continues to obey Eq. 7. This means that the ensemble average pulse shape is unaffected by temperature, for both ordered and disordered chains, agreeing with our simulation results in Fig. 3 for the ordered chain. For any particular member of the ensemble, the mode  $\mu$  has energy  $\frac{1}{2} \omega_{\mu}^2 A_{\mu}^2$  before pulse insertion, and  $\frac{1}{2} \omega_{\mu}^2 (A_{\mu} + \Delta A_{\mu})^2$  after. Using Eq. 6, this can be written as

$$\begin{aligned} E_{\mu}^{\text{before}} &= [f_{\mu} + i g_{\mu} v_0] [f_{\mu}^* - i g_{\mu} v_0] \\ E_{\mu}^{\text{after}} &= [f_{\mu} + i g_{\mu} (v_0 + \Delta v_0)] [f_{\mu}^* - i g_{\mu} (v_0 + \Delta v_0)], \end{aligned} \quad (8)$$

where

$$f_{\mu} = \sqrt{\frac{1}{2N}} \left[ \sum_{\ell}^{\neq 0} \sqrt{M_{\ell}} (\omega_{\mu} u_{\ell} + i v_{\ell}) \mu_{\ell} + \sqrt{M_0} \omega_{\mu} u_0 \mu_0 \right] \quad (9)$$

$$\text{and } g_{\mu} = \sqrt{\frac{M_0}{2N}} \mu_0. \quad (10)$$

The point of Eq. 8 is to separate the coordinate  $v_0$  or  $v_0 + \Delta v_0$  from the remaining coordinates  $u_{\ell}, v_{\ell}$  which are collected in  $f_{\mu}$ . This enables ensemble averages to be done using the fact that  $\langle f_{\mu} v_0 \rangle_T = \langle f_{\mu} \rangle_T \langle v_0 \rangle_T = 0$  and

$\langle f_\mu \Delta v_0 \rangle_T = \langle f_\mu \rangle_T \langle \Delta v_0 \rangle_T = 0$ . The null values follow from the fact that  $\langle f_\mu \rangle_T = 0$ . Note that  $\langle \Delta v_0 \rangle_T \neq 0$ ;  $\Delta v_0$  is chosen to make the V1 pulse have a fixed energy  $E_{\text{pulse}}$ , for every member of the ensemble. This requires

$$\frac{1}{2} M_0 [(v_0 + \Delta v_0)^2 - v_0^2] = E_{\text{pulse}}^{\text{V1}} \quad (11)$$

whether ensemble-averaged or not. This is the general version of the  $T = 0$  form in Eq. 7 which has  $v_0 = 0$ . From Eq. 8 we get

$$\Delta E_\mu^{\text{V1}} = g_\mu^2 [(v_0 + \Delta v_0)^2 - v_0^2] - i(f_\mu - f_\mu^*) g_\mu \Delta v_0. \quad (12)$$

The ensemble average is

$$\langle \Delta E_\mu^{\text{V1}} \rangle_T = g_\mu^2 \langle [(v_0 + \Delta v_0)^2 - v_0^2] \rangle_T. \quad (13)$$

Finally, using Eqs. 7, 10, and 11, we get

$$\langle \Delta E_\mu^{\text{V1}} \rangle_T = E_{\text{pulse}}^{\text{V1}} \frac{\mu_0^2}{N}, \text{ and } \sum_\mu \langle \Delta E_\mu^{\text{V1}} \rangle_T = E_{\text{pulse}}^{\text{V1}}. \quad (14)$$

This proof is sufficiently tedious that the corresponding proofs for V2 and D pulses have not been checked. The results of Fig. 3 indicate that probably all pulses on harmonic chains have shapes independent of  $T$  after ensemble averaging.

## II. NUMERICAL COMPUTATION OF $\Delta E(k, \omega)$

The local energy in Fourier space is

$$\Delta E(k, \omega) = \sum_Q \hbar \omega_Q \Phi_Q(k, \omega), \quad (15)$$

where  $\Phi(k, \omega)$  was derived from Boltzmann theory in relaxation time approximation (RTA):

$$\Phi_Q(k, \omega) = \frac{-i(kv_Q - \omega) \frac{\partial n_Q}{\partial T} \Delta T(k, \omega) + \Delta E_Q^{\text{ext}} / \hbar \omega_Q}{1/\tau_Q + i(kv_Q - \omega)}. \quad (16)$$

The extra equation needed to eliminate the unknown  $\Delta T(k, \omega)$  has two forms,

$$(1) \sum_Q \frac{\hbar \omega_Q \Phi_{Q, \text{RTA}}}{\tau_Q} = 0; \text{ or } (2) \sum_Q \hbar \omega_Q \Phi_{Q, \text{RTA}} = 0. \quad (17)$$

In the appendix of the main paper, these results are used to derive the following

$$\Delta E_{(1)}(k, \omega) = C(k, \omega) \frac{A(k, \omega)}{B(k, \omega)} + D(k, \omega), \quad (18)$$

and

$$\Delta E_{(2)}(k, \omega) = \frac{D(k, \omega)}{F(k, \omega)}, \quad (19)$$

Equations for  $A(k, \omega), \dots, F(k, \omega)$  are in that appendix. Here we convert them to dimensionless functions in dimensionless variables  $x = kv_M / \omega_M = ka/2$ ,  $y = \omega / \omega_M$ , and  $z = Qa/2$ . The definitions are

$$\begin{aligned} A(k, \omega) &= \frac{8E_0}{3N} a(x, y), \\ B(k, \omega) &= \omega_M b(x, y), \\ C(k, \omega) &= c(x, y), \\ D(k, \omega) &= \frac{8E_0}{3N\omega_M} d(x, y), \\ F(k, \omega) &= f(x, y) \end{aligned} \quad (20)$$

The local energy density in the two versions is

$$\Delta E_{(1)}(x, y) = \left( \frac{8E_0/3N}{\omega_M} \right) \left[ \frac{a(x, y)}{b(x, y)} c(x, y) + d(x, y) \right]. \quad (21)$$

$$\Delta E_{(2)}(x, y) = \left( \frac{8E_0/3N}{\omega_M} \right) \frac{d(x, y)}{f(x, y)}. \quad (22)$$

The dimensionless functions of  $(x, y)$  are

$$a(x, y) = \frac{1}{\pi} \int_{-\pi/2}^{\pi/2} dz \frac{\sin^4 z}{1 - \frac{i \cos z}{\epsilon \sin^2 z} (y - x \cos z \text{sign}(z))}, \quad (23)$$

$$b(x, y) = \frac{1}{\pi} \int_{-\pi/2}^{\pi/2} dz \frac{-i(y - x \cos z \text{sign}(z))}{1 - \frac{i \cos z}{\epsilon \sin^2 z} (y - x \cos z \text{sign}(z))}, \quad (24)$$

$$c(x, y) = \frac{1}{\pi} \int_{-\pi/2}^{\pi/2} dz \frac{1}{1 - \frac{i \cos z}{\epsilon \sin^2 z} (y - x \cos z \text{sign}(z))}, \quad (25)$$

$$d(x, y) = \frac{1}{\epsilon \pi} \int_{-\pi/2}^{\pi/2} dz \frac{\cos z \sin^2 z}{1 - \frac{i \cos z}{\epsilon \sin^2 z} (y - x \cos z \text{sign}(z))}. \quad (26)$$

$$f(x, y) = \frac{1}{\pi} \int_{-\pi/2}^{\pi/2} dz \frac{-i(y - x \cos z \text{sign}(z))}{\frac{\epsilon \sin^2 z}{\cos z} - i(y - x \cos z \text{sign}(z))}. \quad (27)$$

For given  $k, \omega$ , the  $z = Qa/2$  integrations often converge fairly slowly. For 80  $Q$ -points (from 0 to  $\pi/a$ ) the error is usually about  $2 - 4 \times 10^{-3}$ , and for 640  $Q$ -points the error is  $\sim 2 \times 10^{-6}$ . Final calculations of these functions of  $(x, y)$  used 1600  $Q$ -points.

## III. NUMERICAL COMPUTATION OF $\Delta E(r, t)$

The Fourier transform needed is

$$\Delta E(r, t) = \frac{16E_0}{3N} \int_{-\infty}^{\infty} \frac{dk}{2\pi} g(k, t) e^{i(2r/a)x}, \text{ where } \quad (28)$$

$$g(k, t) = \int_{-\infty}^{\infty} \frac{dy}{2\pi} h(x, y) e^{-i(\omega_M t)y}, \quad (29)$$

and  $h = (a/b)c + d$  or  $h = d/f$  in cases (1) and (2) respectively. Since  $h(x, -y) = h^*(x, y)$ , Eq. 29 can be simplified to

$$g(x, t) = \frac{1}{\pi} \int_0^{\infty} dy \mathcal{R}e \left\{ e^{-i(\omega_M t)y} h(x, y) \right\}. \quad (30)$$

Since  $g(x, t)$  is even in  $x$ , Eq. 28 can be simplified to

$$\Delta E(r, t) = \frac{16E_0}{3\pi} \int_0^{\infty} dx \cos[(2r/a)x] g(x, t) \quad (31)$$

This shows that  $\Delta E(r, t)$  is real, as physically required.

We need to evaluate  $\Delta E(r, t)$  for  $r$ -values  $na$ ,  $n = 0, 1, \dots, 40$  and for  $t = 80/\omega_M = 40$  in units  $\sqrt{(M/K)}$ . The factor  $h(x, y)$  varies over a wide range of  $x, y$  or  $k, \omega$ , but does not vary too rapidly within the relevant decades of  $(x, y)$ . However, the Fourier factors  $\exp(ikr - i\omega t)$  can vary enormously over a decade of  $x$  or  $y$ . A way to integrate efficiently is to use logarithmic grids for  $x$  and  $y$ , with  $n_g$  points per decade, and  $n_d \sim 10$  decades. We used  $n_g = 500$  for the  $y = \omega/\omega_M$  integral and integrated  $y$  from  $10^{-8}$  to  $10^5$ . For the  $x = ka/2$  integrals we used  $n_g = 40$  points per decade, and integrated from  $x = 10^{-7}$  to  $x = 10^4$ . Between grid points,  $h(x, y)$  is interpolated linearly, and the integration is done exactly

with linearized  $h$ . For example, consider the  $y$  integration of Eq. 30,

$$g(x, t) = \sum_{n=0}^{n_d \times n_g} \Delta g_n \quad (32)$$

$$\Delta g_n \equiv \frac{1}{\pi} \mathcal{R}e \int_{y_n}^{y_{n+1}} dy e^{-i(\omega_M t)y} h(x, y), \quad (33)$$

with  $y_{n+1} = r_y y_n$  and  $(r_y)^{500} = 10$ . In the interval  $(y_n, y_{n+1})$ , approximate  $h(x, y)$  by a linear interpolation:

$$h(x, y_n) + (y - y_n) \left[ \frac{h(x, y_{n+1}) - h(x, y_n)}{y_{n+1} - y_n} \right]. \quad (34)$$

The linearized integral in Eq. 34 is

$$\begin{aligned} & \pi \Delta g_n(x = ka/2, t) \\ & \approx \frac{1}{-i\omega_M t} \left[ e^{-i(\omega_M t)y_{n+1}} h(x, y_{n+1}) - e^{-i(\omega_M t)y_n} h(x, y_n) \right] \\ & - \left( \frac{1}{-i\omega_M t} \right)^2 \left[ e^{-i(\omega_M t)y_{n+1}} - e^{-i(\omega_M t)y_n} \right] \\ & \times \frac{h(x, y_{n+1}) - h(x, y_n)}{y_{n+1} - y_n}. \end{aligned} \quad (35)$$